





Effective yet reliable computation of hyperfine coupling constants in solution by a QM/MM approach: Interplay between electrostatics and non-electrostatic effects

Cite as: J. Chem. Phys. **150**, 124102 (2019); <https://doi.org/10.1063/1.5080810>

Submitted: 12 November 2018 . Accepted: 25 February 2019 . Published Online: 25 March 2019

Tommaso Giovannini , Piero Lafiosca, Balasubramanian Chandramouli , Vincenzo Barone , and Chiara Cappelli 



View Online



Export Citation



CrossMark

ARTICLES YOU MAY BE INTERESTED IN

Perspective: Computational chemistry software and its advancement as illustrated through three grand challenge cases for molecular science

The Journal of Chemical Physics **149**, 180901 (2018); <https://doi.org/10.1063/1.5052551>

Ab initio quantum mechanics/molecular mechanics method with periodic boundaries employing Ewald summation technique to electron-charge interaction: Treatment of the surface-dipole term

The Journal of Chemical Physics **150**, 124103 (2019); <https://doi.org/10.1063/1.5048451>

An extension of the fewest switches surface hopping algorithm to complex Hamiltonians and photophysics in magnetic fields: Berry curvature and “magnetic” forces

The Journal of Chemical Physics **150**, 124101 (2019); <https://doi.org/10.1063/1.5088770>

Lock-in Amplifiers
... and more, from DC to 600 MHz



Effective yet reliable computation of hyperfine coupling constants in solution by a QM/MM approach: Interplay between electrostatics and non-electrostatic effects

Cite as: *J. Chem. Phys.* **150**, 124102 (2019); doi: [10.1063/1.5080810](https://doi.org/10.1063/1.5080810)

Submitted: 12 November 2018 • Accepted: 25 February 2019 •

Published Online: 25 March 2019







View Online



Export Citation



CrossMark

Tommaso Giovannini,^{1,a)}  Piero Lafiosca,¹ Balasubramanian Chandramouli,^{1,2}  Vincenzo Barone,¹ 
and Chiara Cappelli^{1,b)} 

AFFILIATIONS

¹Scuola Normale Superiore, Piazza dei Cavalieri 7, 56126 Pisa, Italy

²Compunet, Istituto Italiano di Tecnologia (IIT), Via Morego 30, 16163 Genova, Italy

^{a)}Electronic mail: tommaso.giovannini@sns.it

^{b)}Electronic mail: chiara.cappelli@sns.it

ABSTRACT

In this paper, we have extended to the calculation of hyperfine coupling constants, the model recently proposed by some of the present authors [Giovannini *et al.*, *J. Chem. Theory Comput.* **13**, 4854–4870 (2017)] to include Pauli repulsion and dispersion effects in Quantum Mechanical/Molecular Mechanics (QM/MM) approaches. The peculiarity of the proposed approach stands in the fact that repulsion/dispersion contributions are explicitly introduced in the QM Hamiltonian. Therefore, such terms not only enter the evaluation of energetic properties but also propagate to molecular properties and spectra. A novel parametrization of the electrostatic fluctuating charge force field has been developed, thus allowing a quantitative reproduction of reference QM interaction energies. Such a parametrization has been then tested against the prediction of EPR parameters of prototypical nitroxide radicals in aqueous solutions.

Published under license by AIP Publishing. <https://doi.org/10.1063/1.5080810>

I. INTRODUCTION

In the last decades, multiscale models have been widely used for the study of molecular properties and spectra.^{1–11} In this context, the most successful approaches fall within the class of “focused models,” which aim at accurately modeling both the physico-chemical properties of the target and its interactions with the surrounding environment. The effect of the latter is seen as a perturbation on the target molecule and is treated at a lower computational level of theory, e.g., by resorting to classical physics, whereas the target molecule is described accurately, generally at the Quantum Mechanical (QM) level. Due to such a partitioning, the computational cost of a QM/classical computation is comparable to that of the corresponding QM isolated system. Such a feature has strongly contributed to the increasing popularity of these models.

QM/Molecular Mechanics (MM) models are among the most renowned classes of QM/classical approaches,^{2,12–18} which have been formalized within different physical frameworks. Beyond the basic mechanical QM/MM embedding, in the last years, much effort has been spent to define electrostatic QM/MM embedding approaches, in which a set of fixed charges is placed on the MM moiety (generally on MM atoms), and the interaction between QM and MM portions is modeled by resorting to the Coulomb law. Clearly, in such approaches, the QM and MM moieties do not mutually polarize. Mutual polarization, i.e., the polarization of the MM portion arising from the interaction with the QM density and vice versa, can be introduced by employing polarizable force-fields, which can be based on distributed multipoles,^{19–23} induced dipoles,^{24–26} Drude oscillators,²⁷ or Fluctuating Charges (FQs).^{8,28,29}

The description of the molecular properties/spectra of embedded systems which is obtained by resorting to polarizable embedding

is generally quite accurate.^{22,25,26,30-32} However, such models are deeply based on the assumption that electrostatic energy terms dominate the target/environment interactions. Non-electrostatic (Pauli repulsion and dispersion) contributions between the QM and MM portions are roughly modeled by using parametrized functions, e.g., the Lennard-Jones potential,^{33,34} which are however completely independent of the QM density. As a result, they are not taken into account in the QM operators so that the calculated spectroscopic/response properties are not affected by such interactions. The reasons why such contributions are generally discarded are connected to the presumption of a numerically dominating effect of electrostatic terms. However, non-electrostatic contributions are crucial to get a physically consistent description of any embedded system, also in the case of target/environment interactions dominated by electrostatics.^{35,36}

A way to include non-electrostatic energy terms is to resort to the Effective Fragment Potential (EFP).^{19,20,37-40} The high accuracy of this method is essentially due to the explicit QM calculation of the molecular orbitals of the environment, drifting apart from the concept at the basis of MM Force Field (FF). A similar QM-based approach, namely, the Polarizable Density Embedding (PDE), has been recently proposed to only include repulsion effects.^{41,42}

A substantially different way of including non-electrostatic interactions in QM/MM approaches consists of exploiting a model recently developed by some of the present authors,⁴³ which formulates repulsion as a function of an auxiliary density on the MM portion and extends the Tkatchenko-Scheffler (TS) approach to density functional theory (DFT)⁴⁴⁻⁴⁸ to treat QM/MM dispersion terms. Notice that the formulation of repulsion contributions in terms of gaussian functions placed in the MM region has also been proposed in the so-called Gaussian Electrostatic Model (GEM).^{36,49-51} However, in both the aforementioned PDE and GEM models, repulsion interaction is modeled as an overlap one-electron integral. Our approach instead defines repulsion contributions in terms of a two-electron exchange integral, thus physically representing the Pauli repulsion. Moreover, differently from the stand-alone approaches discussed above (EFP, PDE, GEM), our approach can easily be coupled to any kind of QM/MM approach because repulsion and dispersion are formulated in a way which is totally independent of the choice of the FF to model the electrostatics (i.e., fixed-charges or polarizable embedding). Remarkably, in our model, repulsion and dispersion contributions are indeed dependent on the QM density. Thus, an explicit contribution to the QM Fock operator exists and the resulting calculated QM properties/spectra are modified by such interactions.

Our model for non-electrostatics in QM/MM has been so far only challenged on reproducing full QM non-electrostatic interaction energies, for which very good results have been obtained.⁴³ In this paper, we start with the extension of the model to spectroscopy. To this end, we report the formulation of non-electrostatic QM/MM terms for EPR, for which environmental effects substantially contribute to the overall observable.⁵²⁻⁵⁴ Environmental (solvent) effects on EPR are usually described by means of continuum models⁵⁵⁻⁵⁸ and only in few cases by adopting electrostatic QM/MM embedding coupled with a classical Molecular Dynamics (MD) to take into account the fluctuations of both the solute conformations and the solvent molecules.⁵⁹⁻⁶⁵

Nitroxide radicals are among the most thoroughly studied radicals from both experimental and computational points of view due to their remarkable stability coupled to strong sensitivity to the polarity of the surrounding and to the pyramidity of the nitrogen atom. Given their importance, several nitroxide radicals have been synthesized to be either used as spin probes (when dispersed in an environment) or as spin labels (when chemically attached to a biological molecule, e.g., a protein).⁶⁶⁻⁶⁸ High-field EPR spectroscopy provides quite rich information consisting essentially of the nitrogen hyperfine and gyromagnetic tensors.⁶⁶ However, interpretation of these experiments in structural terms strongly benefits from quantum mechanical calculations able to dissect the overall observables in terms of the interplay of several subtle effects.^{59,60,69-75} This situation has prompted us to perform a comprehensive study of prototypical nitroxide radicals in aqueous solution coupling density functional and coupled cluster quantum mechanical computations to molecular dynamics simulations, and average of properties for a sufficient number of snapshots including electrostatic, induction, repulsion, and dispersion interactions with the surrounding evaluated by effective quantum mechanical approximations.

To the best of our knowledge, this work presents the first formulation and application of a QM/MM approach accounting at the same time for polarization and non-electrostatic interactions on EPR Hyperfine Coupling Constant (hcc).

The paper is organized as follows: first, the theoretical model is presented. Then, the computational approach is applied to the calculation of hcc_N of two nitroxyl radicals (PROXYL and TEMPO) in aqueous solution. Such compounds are characterized by the presence of the N–O group, which has been most widely used as “spin probe” and “spin label” for the study of structure and dynamics of macromolecular systems.⁶⁶⁻⁶⁸ Summary and Conclusions end the manuscript.

II. THEORETICAL MODEL

The total energy of a system composed by two interacting moieties, one described at the QM level and the other at the MM level, can be expressed as^{76,77}

$$E_{QM/MM} = E_{QM/MM}^{ele} + E_{QM/MM}^{pol} + E_{QM/MM}^{ex-rep} + E_{QM/MM}^{dis}, \quad (1)$$

where $E_{QM/MM}^{ele}$ accounts for electrostatic interactions and $E_{QM/MM}^{pol}$ is the polarization contribution. Such energy terms are those modeled in the electrostatic embedding approach and, in particular, in polarizable QM/MM methods.^{2,12,24-27,78} $E_{QM/MM}^{ex-rep}$ is the exchange-repulsion contribution and $E_{QM/MM}^{dis}$ arises from dispersion interactions.

In this work, electrostatic and polarization terms are modeled by exploiting the Fluctuating Charge (FQ) force field,^{8,30,78-82} whereas non-electrostatic interactions (i.e., the sum of $E_{QM/MM}^{ex-rep}$ and $E_{QM/MM}^{dis}$) are modeled by using the model described in Ref. 43. In the next paragraphs, the mathematical formulation of the different energy contributions is discussed.

A. Electrostatic and polarization interactions

In order to model electrostatic and polarization terms [see Eq. (1)], a polarizable QM/MM embedding needs to be adopted.

In such a model, the MM force field adapts to the external field/potential originating from the QM density and electrostatic/polarization terms are included in the QM Hamiltonian, so as to describe the mutual interaction between the QM density and the environment.

In this work, we will resort to the FQ force field.⁸ In the resulting QM/FQ model, the electrostatic potential due to the QM density together with the differences in electronegativities between different atoms in the MM region gives rise to a charge fluctuation in the MM region, up to the point that the differences in electrochemical potential between the MM atoms vanish. From a mathematical point of view, this results in the following linear equation:⁸³

$$\mathbf{D}\mathbf{q}_\lambda = -\mathbf{C}_Q - \mathbf{V}(\mathbf{P}_{QM}), \quad (2)$$

where \mathbf{D} is a response matrix, whose diagonal terms are atomic chemical hardnesses and \mathbf{q} is a vector containing the FQs and Lagrangian multipliers. \mathbf{C} contains atomic electronegativities and those constraints which are needed to ensure each MM molecule has a fixed charge. $\mathbf{V}(\mathbf{P})$ is the potential due to the QM density matrix \mathbf{P} calculated at MM charges positions. We refer the reader to Ref. 84 for further details.

The interaction between FQ charges and the QM density obeys the Coulomb law,

$$E_{QM/MM}^{ele} + E_{QM/MM}^{pol} = \sum_{j=1}^{N_{FQs}} \int_{\mathbf{R}^3} \frac{\rho_{QM}(\mathbf{r})q_j}{|\mathbf{r} - \mathbf{r}_j|} d\mathbf{r}. \quad (3)$$

By differentiating Eq. (3) with respect to the density matrix, $P_{\mu\nu}$, the contribution to the Fock matrix is obtained,⁸³

$$F_{\mu\nu} = \frac{\partial E}{\partial P_{\mu\nu}} = \mathbf{V}_{\mu\nu}^\dagger \mathbf{q}. \quad (4)$$

The Fock matrix defined in this way can enter a SCF procedure, so as to finally give a QM density mutually equilibrated with the FQs.

B. Pauli repulsion energy

The exchange-repulsion energy, $E_{QM/MM}^{ex-rep}$, also known as Pauli repulsion energy, is formally due to the Pauli principle, i.e., wavefunction antisymmetry. From a mathematical point of view, it can be formulated as the opposite of an exchange integral,^{77,85}

$$E_{QM/MM}^{ex-rep} = \frac{1}{2} \int \frac{d\mathbf{r}_1 d\mathbf{r}_2}{r_{12}} \rho_{QM}(\mathbf{r}_1, \mathbf{r}_2) \rho_{MM}(\mathbf{r}_2, \mathbf{r}_1). \quad (5)$$

In order to define the density matrix ρ_{MM} , we localize fictitious valence electron pairs for MM molecules in bond and lone pair regions and represent them by s-gaussian-type functions. The expression for ρ_{MM} becomes

$$\rho_{MM}(\mathbf{r}_1, \mathbf{r}_2) = \sum_{\mathbf{R}} \xi_{\mathbf{R}}^2 e^{-\beta_{\mathbf{R}}(\mathbf{r}_1 - \mathbf{R})^2} \cdot e^{-\beta_{\mathbf{R}}(\mathbf{r}_2 - \mathbf{R})^2}, \quad (6)$$

where \mathbf{R} collects the centers of the gaussian functions used to represent the fictitious MM electrons. The β and ξ parameters are generally different for lone-pairs or bond-pairs, their values being adjusted

to the specific kind of environment (MM portion) to be modeled. By substituting Eq. (6) in Eq. (5), the QM/MM repulsion energy reads

$$E_{QM/MM}^{rep} = \frac{1}{2} \sum_{\mathbf{R}} \int \frac{d\mathbf{r}_1 d\mathbf{r}_2}{r_{12}} \rho_{QM}(\mathbf{r}_1, \mathbf{r}_2) \cdot \left[\xi_{\mathbf{R}}^2 e^{-\beta_{\mathbf{R}}(\mathbf{r}_1 - \mathbf{R})^2} \cdot e^{-\beta_{\mathbf{R}}(\mathbf{r}_2 - \mathbf{R})^2} \right]. \quad (7)$$

It is worth noticing that in this formalism, QM/MM Pauli repulsion energy is calculated as a two-electron integral. Equation (7) is general enough to hold for any kind of MM environment (solvents, proteins, surfaces, etc.). The nature of the external environments is specified by defining the number of different electron-pair types and the corresponding β and ξ parameters in Eq. (6). Also, the formalism is general so that it can be coupled to any kind of QM/MM approach.

By differentiating Eq. (7) with respect to the density matrix, the corresponding contribution to the Fock matrix is obtained,

$$F_{\mu\nu}^{rep} = \frac{\partial E^{rep}}{\partial P_{\mu\nu}} = \frac{1}{2} \int d\mathbf{r}_1 \left[\frac{\chi_\mu(\mathbf{r}_1)A_\nu(\mathbf{r}_1) + A_\mu(\mathbf{r}_1)\chi_\nu(\mathbf{r}_1)}{2} \right], \quad (8)$$

where χ_μ are atomic basis functions and A_μ are calculated as detailed in Ref. 43.

C. Quantum dispersion energy

To formulate dispersion interactions, we start from the Tkatchenko and Scheffler (TS) DFT functional. In this model, the dispersion energy can be written as

$$E^{dis} = -\frac{1}{2} \sum_{A,B} f_{damp}(R_{AB}, R_A^0, R_B^0) C_{6AB} R_{AB}^{-6}, \quad (9)$$

where R_{AB} is the distance between atoms A and B in a given system, C_{6AB} is the corresponding C_6 coefficient, R_A^0 and R_B^0 are their van der Waals (vdW) radii. The R_{AB}^{-6} singularity at small distances is eliminated by the short-range damping function $f_{damp}(R_{AB}, R_A^0, R_B^0)$.⁴⁴

C_{6AB} coefficients can be expressed in terms of homonuclear parameters C_{6AA} , C_{6BB} , which in turn can be obtained through an Hirshfeld⁸⁶ partition of the density.⁴⁴ Notice that alternative partitioning approaches can in principle be exploited.⁸⁷

Such an approach can be reformulated within a QM/MM formalism,^{43,48} yielding

$$E_{QM/MM}^{dis} = -\frac{1}{2} \sum_{A \in QM} \sum_{B \in MM} f_{damp}(R_{AB}, R_A^0, R_B^0) \cdot \frac{\eta_A^2 C_{AA}^{free} C_{BB}^{eff}}{\frac{\alpha_B^0}{\alpha_A^0} \eta_A^2 C_{AA}^{free} + \frac{\alpha_A^0}{\alpha_B^0} C_{BB}^{eff}} R_{AB}^{-6}, \quad (10)$$

where C_{6BB}^{eff} are effective homonuclear coefficients of B (MM) atoms and C_{6AA}^{free} are free homonuclear coefficients of A QM atoms. α_A^0 and α_B^0 are static dipole polarizabilities, whereas η_A is a function converting C_{6AA}^{free} into C_{6AA}^{eff} . Further details can be found in Refs. 43, 44, and 48.

$f_{damp}(R_{AB}, R_A^0, R_B^0)$ in Eq. (10) is a Fermi-type damping function,^{44,88,89}

$$f_{damp}(R_{AB}, R_A^0, R_B^0) = \frac{1}{1 + \exp\left[-d\left(\frac{R_{AB}}{s_R R_{AB}^0} - 1\right)\right]}, \quad (11)$$

where $R_{AB}^0 = R_A^0 + R_B^0$, and d and s_R are free parameters.

Similarly to what has already been done for electrostatic and repulsion contributions, by differentiating Eq. (10) with respect to the QM density matrix, the dispersion contribution to the Fock matrix is obtained,⁴³

$$F_{\mu\nu}^{dis} = -\frac{1}{2} \sum_{A \in \text{QM}} \sum_{B \in \text{MM}} f_{damp}(R_{AB}) \cdot \frac{2 \frac{\alpha_A^0}{\alpha_B^0} C_{6BB}^2 C_{6AA}^{free} 2\eta_A}{\left(\frac{\alpha_A^0}{\alpha_A^0} C_{6AA}^{eff} + \frac{\alpha_B^0}{\alpha_B^0} C_{6BB}\right)^2} \eta_{A,\mu\nu}^{\rho} R_{AB}^{-6}. \quad (12)$$

The complete derivation and definition of $\eta_{A,\mu\nu}^{\rho}$ can be found in Ref. 43.

D. Hyperfine coupling constant

The spin Hamiltonian describing the interaction between the electron spin (S) of a free radical containing a magnetic nucleus of spin I and an external magnetic field (B) can be written as

$$H_S = \mu_B \vec{S} \cdot \mathbf{g} \cdot \vec{B} + \frac{1}{\hbar \gamma_I} \vec{S} \cdot \mathbf{A} \cdot \vec{\mu}_I, \quad (13)$$

where the first term is the Zeeman interaction between the electron spin and the external magnetic field through the Bohr magneton μ_B and $\mathbf{g} = g_e \mathbf{1}_3 + \Delta \mathbf{g}_{corr}$. $\Delta \mathbf{g}_{corr}$ accounts for the correction to the free electron value ($g_e = 2.0022319$) due to several terms including the relativistic mass ($\Delta \mathbf{g}_{RM}$), the gauge first-order corrections ($\Delta \mathbf{g}_C$), and a term arising from the coupling of the orbital Zeeman (OZ) and the spin-orbit coupling (SOC) operator.^{90,91} The second term on the rhs of Eq. (13) describes the hyperfine interaction between S and the nuclear spin I through the hyperfine coupling tensor \mathbf{A} . The latter, which is defined for each nucleus X , can be decomposed into two terms,

$$\mathbf{A}(X) = A_X \mathbf{1}_3 + \mathbf{A}_{dip}(X). \quad (14)$$

The dipolar term $\mathbf{A}_{dip}(X)$ is a zero-trace tensor, whose contribution vanishes in isotropic media (e.g., solutions). The first term A_X (Fermi-contact interaction), which is an isotropic contribution, is also known as hyperfine coupling constant (hcc). It is related to the spin density (ρ_X) at nucleus X by the following relation:

$$A_X = \frac{4\pi}{3} \mu_B \mu_X g_e g_X \langle S_Z \rangle^{-1} \rho_X^{\alpha-\beta}, \quad (15)$$

where $\rho_X^{\alpha-\beta}$ can be obtained as

$$\rho_X^{\alpha-\beta} = \sum_{\mu\nu} P_{\mu\nu}^{\alpha-\beta} \langle \chi_{\mu}(\mathbf{r}) | \delta(\mathbf{r} - \mathbf{r}_X) | \chi_{\nu}(\mathbf{r}) \rangle. \quad (16)$$

$P^{\alpha-\beta}$ is the difference between α and β density matrices. Because in our approach both electrostatic and non-electrostatic dispersion/repulsion interactions enter the definition of the QM Fock operators [see Eqs. (4), (8), and (12)], $P^{\alpha-\beta}$ is modified. Therefore, hyperfine coupling constants with the account of electrostatic, polarization, dispersion, and repulsion QM/MM interactions are obtained.

III. COMPUTATIONAL DETAILS

Molecular geometries of PROXYL and TEMPO radicals (Fig. 1) were optimized *in vacuo* by combining B3LYP and PBE0 hybrid density functionals with both aug-cc-pVDZ and 6-311++G(3df,2pd) basis sets. For all optimized structures, the hyperfine coupling constant of nitrogen atom was calculated by exploiting both B3LYP and PBE0 and the N07D basis set.^{92,93} For the sake of comparison, on the reduced structures depicted in Fig. 1, which are obtained by removing ring atoms for both TEMPO and PROXYL but keeping fixed all the geometrical parameters, additional coupled-cluster single double (CCSD)/EPR-II⁹⁴ calculations were performed.

Clusters made of TEMPO and PROXYL radicals with two explicit water molecules (see Fig. 3) were optimized at the PBE0/6-311++G(3df,2pd) level, according to previous studies.⁵⁷ For those structures, the interaction energy between the radicals and the two water molecules was computed by exploiting SAPT0/aug-cc-pVTZ or jun-cc-pVDZ or N07D (as implemented in Psi4 1.1⁹⁵) and CCSD(T)/aug-cc-pVTZ, jun-cc-pVDZ, and N07D. Counterpoise corrections were included in CCSD(T) calculations. QM/MM energy calculations were also performed at the PBE0/aug-cc-pVTZ, jun-cc-pVDZ, and PBE0/N07D level, by including dispersion and repulsion energies obtained by exploiting our model.⁴³ The QM portion was restricted to the radical, whereas the two water molecules were treated at the MM level. The MM region was described by means of a non-polarizable force field (TIP3P⁹⁶) and the polarizable FQ approach^{8,78} by exploiting two literature parametrizations^{28,97} and a new parametrization proposed in this work. The parameters used for modeling dispersion and repulsion interactions were taken from Ref. 43. On the same structures, full QM and QM/MM nitrogen hyperfine coupling constants were calculated by exploiting the PBE0/N07D level of theory for treating the QM portion. For the sake of comparison, on the reduced cluster structures depicted in Fig. 3, which are obtained by removing ring

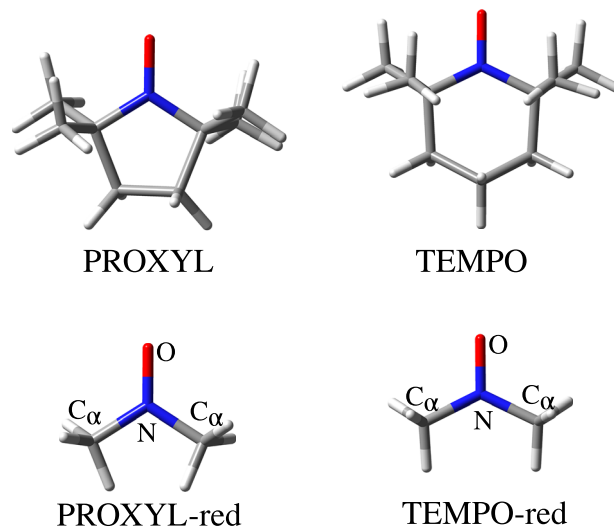


FIG. 1. Top: PROXYL and TEMPO structures. Bottom: reduced structures used for CCSD/EPR-II calculations.

atoms for both TEMPO and PROXYL but keeping fixed all the geometrical parameters, additional CCSD/EPR-II⁹⁴ hcc_N calculations were performed.

Classical MD simulations were performed with the Amber software (v.12) using the ff99SB force field.^{98,99} Parameters for nitroxides were obtained from a previous study by one of the present authors.⁵⁹ The nitroxides were embedded in a cubic box of TIP3P water molecules, which extended to 30 Å from the solute surface. The starting systems were equilibrated following a multistep protocol: (i) minimization of the whole system for 10 000 steps, (ii) heating of the system from 103 to 303 K in 100 ps with a mild restraint of 0.5 kcal/mol Å² on the solute, and (iii) equilibration in NPT ensemble at a pressure of 1 bar and 303 K for 100 ps. The production phase was then initiated in NVT ensemble and continued for 10 ns. The simulation conditions involved Periodic Boundary Condition (PBC), a 1 fs time step for numerical integration, using SHAKE for constraining bonds involving hydrogen atoms,¹⁰⁰ a 10 Å cut-off for non-bonded interactions, particle mesh ewald (PME) for evaluating the long-range electrostatics,¹⁰¹ temperature regulation with Langevin coupling using a collision frequency of 1.0 ps⁻¹, and snapshot collection in the trajectory at 1 ps interval.

A total of 200 uncorrelated snapshots were extracted from the MDs (one snapshot every 50 ps). For each snapshot, a 13 Å sphere centered at the solute's geometric center was cut. All hyperfine coupling constants were calculated within the QM/FQ or QM/TIP3P framework at the PBE0/N07D level. The FQ water molecules were modeled both with the SPC FQ parameters,²⁸ the parametrization proposed by some of the present authors,⁹⁷ and the parameters proposed in this work. The convergence of the hcc_N values with increasing number of representative snapshots was checked for both radicals. Dispersion and repulsion contributions to hcc_N were included by exploiting what has been explained in Secs. II B and II C. All QM/FQ calculations were performed by using a locally modified version of Gaussian 16.¹⁰² Finally, the calculated values were compared with the experimental data taken from Refs. 103 and 104.

IV. NUMERICAL RESULTS

In this section, we will report the results issuing from the application of the developed methodology to the calculation of the nitrogen hyperfine coupling constant (hcc_N) of PROXYL and TEMPO radicals in aqueous solution. In order to evaluate the role of the different terms (electrostatic/polarization/dispersion/repulsion) concurring with the overall solvent effect, we will present the results obtained by exploiting a hierarchy of different approaches, starting from a simple cluster model (isolated radical plus two water molecules) to averaging over a set of representative structures extracted from MD runs, with or without the inclusion of polarization/dispersion/repulsion solvent contributions. In addition, to allow a direct comparison with experimental hcc_N , reference values for the isolated radicals are discussed.

A. hcc_N of isolated radicals

PROXYL and TEMPO geometries (see Fig. 1) were optimized *in vacuo* at different levels of theory. In particular, B3LYP

and PBE0 functionals in combination with aug-cc-pVDZ (BS1) or 6-311++G(3df,2pd) (BS2) basis sets were employed. Selected geometrical parameters are reported in Table I. In particular, the N-O distance, the $C_\alpha NC_\alpha$ angle, and the improper dihedral angle $C_\alpha NOC_\alpha$ were taken into consideration (see Fig. 1 for atom labeling). Additional data obtained with B3LYP-D3 and PBE0-D3 functionals⁹⁸ can be found in Table S1 given as supplementary material. Geometries were also optimized by exploiting the B2PLYP double hybrid functional combined with the maug-cc-pVTZ-d(H) basis set (BS3), which has been reported to reliably describe molecular geometries.¹⁰⁵ The values reported in Table I clearly show that B3LYP/aug-cc-pVDZ and B2PLYP/maug-cc-pVTZ-d(H) perform in a similar way. However, all the considered combinations of functional and basis set do not differ much from the best calculated structure of both radicals. It is worth pointing out that the most relevant difference between PROXYL and TEMPO stands in the value of the improper dihedral angle $C_\alpha NOC_\alpha$, which is related to the nitrogen atom pyramidalization. In fact, the angle is almost zero for PROXYL and about -21° for TEMPO.

For all the optimized structures obtained with PBE0 and B3LYP functionals in conjunction with BS1 and BS2, hcc_N were calculated by exploiting either PBE0 or B3LYP and the N07D basis sets purposely parametrized for both functionals (see Refs. 92 and 93 for more details). For the sake of comparison, additional hcc_N calculations were performed at the CCSD/EPR-II⁹⁴ level on the reduced structures depicted at the bottom of Fig. 1. All results are reported in Table II.

hcc_N for the two radicals differ by about 3 gauss at all levels. Such differences are essentially due to the different pyramidalization of the nitroxyl group. The small discrepancies which are reported for the various optimized structures are due to small fluctuations in the improper dihedral angle (see Table I). Notice that all calculated DFT hcc_N are underestimated with respect to CCSD/EPR-II values.

To further investigate on the role of nitrogen pyramidalization on hcc_N , PBE0/N07D hcc_N values for the reduced TEMPO structure as a function of $C_\alpha NOC_\alpha$ were calculated. The data are graphically reported in Fig. 2.

As it can be noticed, the value computed for PROXYL and TEMPO radicals is almost recovered at zero and $\pm 20^\circ$, respectively. For larger $C_\alpha NOC_\alpha$ values, computed hcc_N values increase up to the maximum value (22 gauss) at about $\pm 40^\circ$. Such a trend confirms

TABLE I. Selected geometrical parameters of PROXYL and TEMPO radicals at the different levels of theory. BS1: aug-cc-pVDZ; BS2: 6-311++G(3dp,2pd); BS3: maug-cc-pVTZ-d(H).

| Parameter | PBE0 | | B3LYP | | B2PLYP |
|-----------------------------|------------|------------|------------|------------|------------|
| | BS1 | BS2 | BS1 | BS2 | BS3 |
| PROXYL | | | | | |
| N-O | 1.262 | 1.257 | 1.274 | 1.268 | 1.273 |
| $\angle C_\alpha NC_\alpha$ | 115.3 | 115.2 | 115.4 | 115.2 | 115.2 |
| $C_\alpha NOC_\alpha$ | ± 0.0 | ± 0.0 | ± 0.0 | ± 0.0 | ± 0.0 |
| TEMPO | | | | | |
| N-O | 1.271 | 1.266 | 1.283 | 1.278 | 1.282 |
| $\angle C_\alpha NC_\alpha$ | 124.1 | 124.2 | 124.5 | 124.6 | 124.4 |
| $C_\alpha NOC_\alpha$ | ± 22.0 | ± 21.3 | ± 21.2 | ± 20.6 | ± 21.6 |

TABLE II. Calculated hcc_N values (Gauss). BS1: aug-cc-pVDZ; BS2: 6-311++G(3dp,2pd).

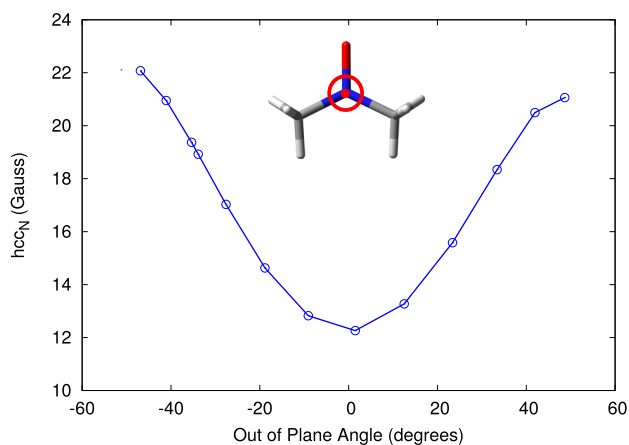
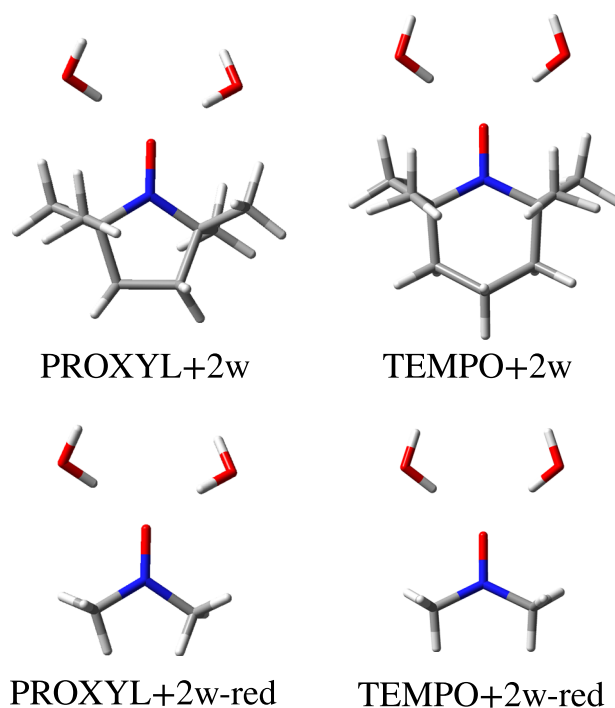
| Radical | Optimized structure | PBE0/N07D | B3LYP/N07D | CCSD/EPR-II |
|-----------|---------------------|-----------|------------|-------------|
| | PROXYL | B3LYP/BS1 | 11.8 | 11.4 |
| B3LYP/BS2 | | 12.0 | 11.3 | 12.6 |
| PBE0/BS1 | | 11.8 | 11.1 | 12.4 |
| PBE0/BS2 | | 11.7 | 11.0 | 12.3 |
| TEMPO | B3LYP/BS1 | 15.0 | 14.4 | 15.9 |
| | B3LYP/BS2 | 14.8 | 14.2 | 15.7 |
| | PBE0/BS1 | 14.9 | 14.3 | 15.7 |
| | PBE0/BS2 | 14.7 | 14.0 | 15.4 |

what has already been reported by one of the present authors.⁶⁰ In Fig. S1 of the [supplementary material](#), we report for comparison CCSD/EPR-II hcc_N values as a function of $C_\alpha NOC_\alpha$. DFT underestimates spin polarization (which is the only relevant contribution for the planar structure) and at the same time overestimates the singly occupied molecular orbital (SOMO) delocalization, which instead increases as the $C_\alpha NOC_\alpha$ increases.

B. hcc_N of PROXYL/TEMPO+water clusters

The most basic method to describe hydrated radicals is to resort to a cluster approach. In particular, due to the presence of the oxygen atom, a natural choice consists of saturating oxygen doublets with two water molecules (see Fig. 3).^{57,60} According to what has already been proposed in previous studies, all structures were optimized at the PBE0/6-311++G(3df,2pd) level.^{57,59}

To quantify the different contributions to the radical/water interaction energy, Energy Decomposition Analysis (EDA) as formulated in the Symmetry-Adapted Perturbation Theory (SAPT0)^{106,107} was performed by exploiting the aug-cc-pVTZ basis set on the reduced structure of the PROXYL cluster (see Fig. 3).

**FIG. 2.** PBE0/N07D hcc_N values (Gauss) on the reduced TEMPO structure as a function of the out of plane $C_\alpha NOC_\alpha$ angle.**FIG. 3.** PBE0/6-311++G(3df,2pd) optimized structures of clusters of PROXYL (top) and TEMPO (bottom) with two water molecules.

Additional SAPT0 calculations were performed by exploiting both the jun-cc-pVDZ and N07D basis sets (see Table S2 given as [supplementary material](#)). Such additional sets were selected because jun-cc-pVDZ has been reported to provide good results for closed shell systems,¹⁰⁸ whereas N07D is exploited in this study to calculate hcc_N .

SAPT0/aug-cc-pVTZ results are reported in Table III, together with the corresponding values obtained by treating the radical at the QM level (PBE0/aug-cc-pVTZ) and the two water molecules at the MM level. QM/MM electrostatic interactions were described by

TABLE III. PROXYL+2w EDA obtained by exploiting PBE0/FQ with different parametrizations and SAPT0. CCSD(T) calculations include counterpoise corrections. All data are reported in mHartree and were obtained by using the aug-cc-pVTZ basis set.

| | FQ ^a | FQ ^b | FQ ^c | SAPT0 | CCSD(T) |
|---------------|-----------------|-----------------|-----------------|--------|---------|
| Electrostatic | -20.60 | -26.80 | -47.06 | -31.35 | ... |
| Induction | ... | ... | ... | -11.45 | ... |
| Repulsion | 27.78 | 28.58 | 30.99 | 28.34 | ... |
| Dispersion | -3.28 | -3.28 | -3.28 | -9.43 | ... |
| Total | 3.90 | -1.50 | -19.35 | -23.89 | -20.62 |

^aFQ parametrization taken from Ref. 28.

^bFQ parametrization taken from Ref. 97.

^cFQ parametrization proposed in this work.

TABLE IV. hcc_N of PROXYL/TEMPO+2w clusters obtained at different levels of theory. All data are reported in gauss.

| | PBE0/N07D | | | | | | | | CCSD/EPR-II | $\Delta_{CC/PBE0}$ | Expt. | | |
|--------|---------------|-----------------|-----------------|-----------------|--|-----------------|-----------------|-----------------|-------------|--------------------|--------------|-----|------|
| | Electrostatic | | | | Electrostatic + Dispersion/ Repulsion | | | | Full-QM | Full-QM(red) | Full-QM(red) | | |
| | TIP3P | FQ ^a | FQ ^b | FQ ^c | TIP3P | FQ ^a | FQ ^b | FQ ^c | | | | | |
| PROXYL | 13.4 | 13.1 | 13.4 | 14.3 | 13.1 | 12.8 | 13.1 | 13.9 | 13.7 | 13.7 | 14.6 | 0.9 | 16.4 |
| TEMPO | 17.9 | 15.3 | 15.7 | 16.7 | 16.9 | 14.8 | 15.1 | 16.1 | 15.9 | 16.3 | 17.1 | 0.8 | 17.3 |

^aFQ parametrization taken from Ref. 28.^bFQ parametrization taken from Ref. 97.^cFQ parametrization proposed in this work

using the FQ approach with three different parametrizations (see Table S3 in the [supplementary material](#)), whereas QM/MM repulsion and dispersion contributions were modeled as reported above. Additional CCSD(T)/aug-cc-pVTZ calculations including counterpoise¹⁰⁹ corrections were also performed to quantify the accuracy of SAPT0 interaction energies.

SAPT0 values show that electrostatic interactions (i.e., the sum of electrostatic and induction terms) give larger contributions with respect to non-electrostatic (repulsion+dispersion). However, non-electrostatic interactions and in particular repulsion cannot be neglected, as it is commonly done in standard QM/MM models.

Moving to QM/FQ, we first notice that the available parametrizations (FQ^a and FQ^b in [Table III](#)) focus on modeling electrostatic interactions; however, they can indeed be inadequate whenever non-electrostatic terms are taken into consideration. This is confirmed by our results ([Table III](#)): FQ^a and FQ^b electrostatic energies give a qualitatively correct description of SAPT0 or CCSD(T) total interaction energies. On the contrary, FQ^a and FQ^b total interaction energies are unsatisfactory; therefore, a novel FQ parametrization is required (labeled FQ^c in [Table III](#)). Differently from FQ^a and FQ^b, which were obtained to reproduce water bulk properties (FQ^a, Ref. 28) or QM atomic charges (FQ^b, Ref. 97), FQ^c is tuned to the total interaction energy at the CCSD(T) level (with an error of less than 1 kcal/mol). FQ^c yields an accurate description of SAPT0 electrostatic interactions. Notice that similar findings are given by both jun-cc-pVDZ and N07D basis sets (see [Table S2](#) in the [supplementary material](#)). To end the discussion on interaction energies, it is worth noticing that the analysis reported above is only allowed when non-electrostatic interactions are included in QM/MM calculations, i.e., it is not achievable by exploiting common purely electrostatic approaches.

Calculated hcc_N of the PROXYL/TEMPO+2w clusters are reported in [Table IV](#). QM/MM calculations were performed by exploiting both the non-polarizable TIP3P⁹⁶ force field and FQ (with different parametrizations) to describe electrostatic interactions. Two set of QM/MM calculations were performed. The first employs TIP3P or FQ embedding and do not include non-electrostatic interactions. The corresponding results are reported in the first four columns of [Table IV](#). In the second set of calculations, non-electrostatic interactions, as obtained with our model, are included. All results are also compared with full QM calculations;

i.e., both the radicals and the two water molecules are described at the QM level (see column 9 in [Table IV](#)).

The reported data clearly show that the non-polarizable TIP3P approach gives large errors with respect to full QM calculations; remarkably, the inclusion of non-electrostatic terms does not improve the results. A different picture results from polarizable QM/FQ values. In fact, when only the electrostatic interactions are considered, the FQ^b parametrization gives values which are in fair agreement with the reference full QM data. However, the inclusion of non-electrostatic interactions shifts hcc_N values in the wrong direction, thus increasing the absolute difference with respect to reference values. This is not surprising because EDA analysis (see [Table III](#)) already showed underestimated electrostatic interactions. The same considerations are also valid for FQ^a, whereas the novel FQ^c parametrization overestimates hcc_N values if only electrostatic interactions are considered. Remarkably, the inclusion of non-electrostatic interactions shifts FQ^c values in the right direction, and the agreement with full QM reference data is almost perfect (0.2 G).

Furthermore, additional PBE0/N07D and CCSD/EPR-II calculations were performed on the reduced structures depicted in [Fig. 3](#) (see [Table IV](#)). Full QM DFT calculations underestimate CCSD/EPR-II hcc_N values by 0.9 and 0.8 G for PROXYL and TEMPO, respectively. Notice that calculated CCSD/EPR-II hcc_N are still not comparable with experimental values, especially for PROXYL. This confirms that the cluster approach is inadequate to physically describe the solvation phenomenon, which is intrinsically a dynamical process.

C. hcc_N of PROXYL/TEMPO from MD runs

An alternative and more accurate way of modeling solvation is to combine our approach with classical MD. [Table V](#) reports selected

TABLE V. Mean values and standard deviations (in brackets) of selected geometrical parameters of PROXYL and TEMPO structures extracted from MD runs.

| | (PROXYL) | (TEMPO) |
|------------------------------|------------------|------------------|
| N–O | 1.27 (0.03) | 1.27 (0.03) |
| $\angle C_\alpha N C_\alpha$ | 115.3 (2.5) | 123.6 (2.7) |
| $C_\alpha N O C_\alpha$ | ± 0.4 (17.8) | ± 5.0 (20.1) |

geometrical parameters (and their standard deviation) obtained by averaging 200 representative snapshots extracted from MD runs performed on PROXYL and TEMPO in aqueous solution. The improper dihedral angle $C_\alpha\text{NOC}_\alpha$, which as stated before plays a crucial role in determining EPR parameters, is drastically different with respect to what has been reported for the isolated radicals, especially for TEMPO. Furthermore, due to the dynamical picture given by the MD, the geometrical parameters are accompanied by standard deviations (in brackets), which are large in the case of this angle.

In order to show how the variability in the improper dihedral affects calculated hcc_N values, two different set of calculations were performed. First, all solvent molecules in all snapshots were removed and hcc_N were calculated on the resulting structures. Second, all solvent molecules were indeed included and treated at the FQ level, with the sole inclusion of electrostatic effects (c parametrization). In Figs. 4 and 5, the resulting hcc_N values are reported as a function of the out-of-plane $C_\alpha\text{NOC}_\alpha$ angle.

As expected, the same picture as already reported for the isolated radicals emerges.

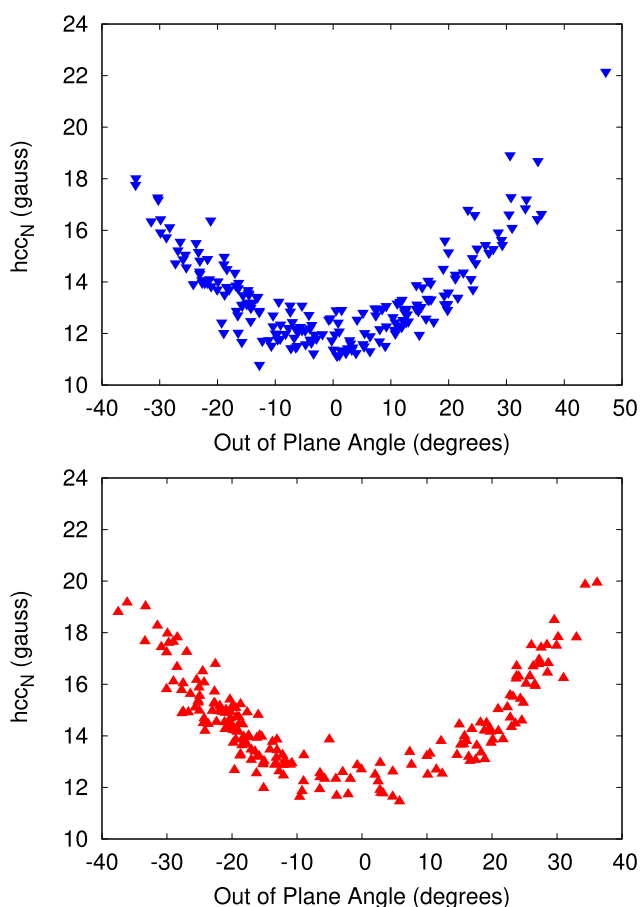


FIG. 4. PBE0/N07D calculated hcc_N (gauss) on the solute-only structures extracted from MD runs as a function of the out of plane $C_\alpha\text{NOC}_\alpha$ angle. (Top: PROXYL; bottom: TEMPO).

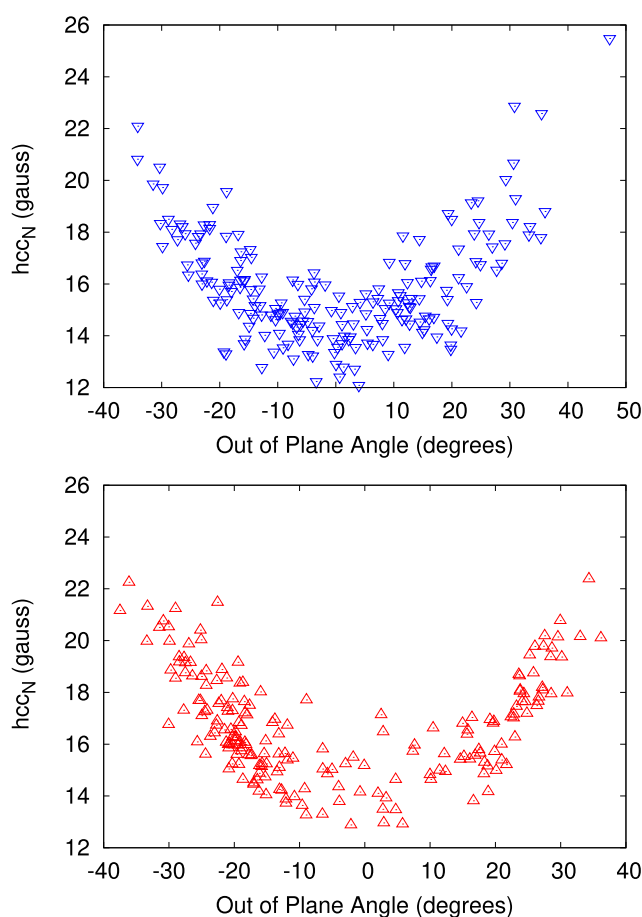


FIG. 5. PBE0/N07D QM/FQ calculated hcc_N (gauss) on the entire snapshots extracted from MD runs as a function of the out of plane $C_\alpha\text{NOC}_\alpha$ angle. (Top: PROXYL; bottom: TEMPO).

Due to the large variability of hcc_N values as a function of the out of plane angle, the convergence of average values needs to be carefully checked. In Fig. 6, QM/FQ hcc_N average values as a function of the number of snapshots are depicted for the two radicals. Clearly, hcc_N is well converged by using 200 snapshots.

Let us now compare our computed data with their experimental counterparts. Table VI collects hcc_N values computed with different approaches. QM indicates calculations performed on the solute-only structures extracted from MD (see above). QM/FQ data were obtained by using the purely electrostatic polarizable FQ with the c parametrization (the results obtained by exploiting the a , b parametrizations are reported in Table S4 in the supplementary material). The contribution to hcc_N due to repulsion interactions is denoted as Δ_{rep} , whereas the contribution to hcc_N of both repulsion and dispersion interactions is denoted as $\Delta_{\text{dis-rep}}$.

We first notice that, due to the different structural sampling given by the MD, the QM data in Table VI differ from what was reported for the isolated radicals (see Table II). The dynamical sampling increases PROXYL and TEMPO hcc_N values by about 2.4

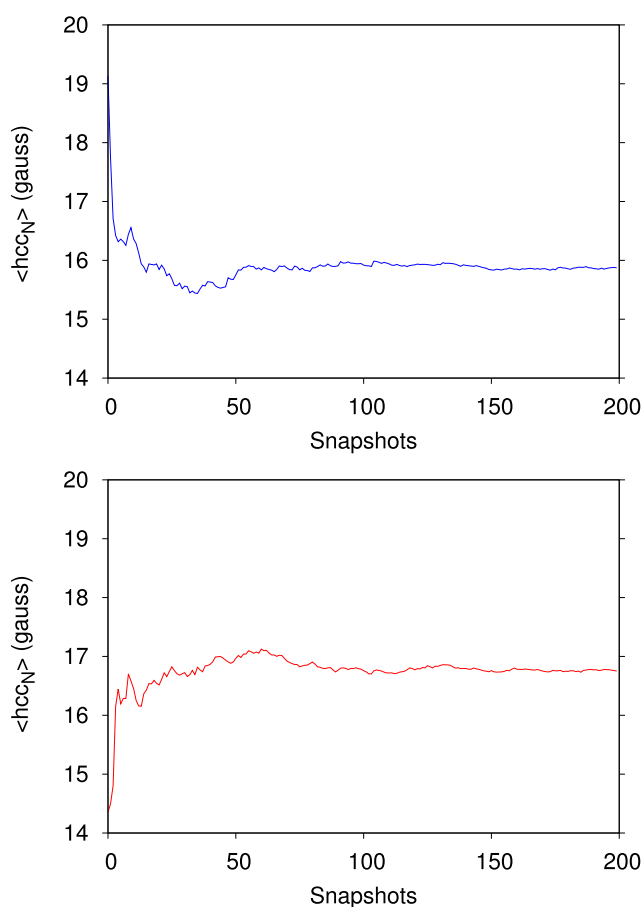


FIG. 6. QM/FQ hcc_N mean value as a function of the number of snapshots extracted from MD runs. (Top: PROXYL; bottom: TEMPO) All data are reported in gauss.

and 2.2 gauss, respectively. As a result, the difference between hcc_N values of the two radicals (1.1 gauss) is in good agreement with experimental data (0.9 G).^{103,104} When full solvent effects are included at the purely electrostatic FQ level (2nd column), hcc_N values are increased by about 2.3 gauss on average for both

TABLE VI. PBE0/N07D hcc_N mean values calculated on 200 snapshots extracted from MD runs. QM indicates the calculation performed on solute-only structures. FQ refers to the purely electrostatic QM/FQ with c parametrization. Δ_{rep} and $\Delta_{\text{dis-rep}}$ are differences between FQ and hcc_N data obtained with our method. Best QM/MM data are obtained by summing FQ, $\Delta_{\text{dis-rep}}$, and $\Delta_{\text{CC/PBE0}}$ (see Table IV). All values are reported in gauss.

| | QM | FQ | Δ_{rep} | $\Delta_{\text{dis-rep}}$ | Best QM/MM FQ + $\Delta_{\text{dis-rep}}$ + $\Delta_{\text{CC/PBE0}}$ | Expt. |
|--------|------|------|-----------------------|---------------------------|--|--------------|
| PROXYL | 13.5 | 15.9 | -0.4 | -0.4 | 16.4 ± 0.1 | 16.4^{103} |
| TEMPO | 14.6 | 16.8 | -0.5 | -0.5 | 17.1 ± 0.1 | 17.3^{104} |

radicals. This means that attractive interactions increase the computed property. As a result, the inclusion of repulsive interaction terms is expected to decrease computed values, and this is indeed confirmed by the values reported in the third column. In particular, for both radicals, hcc_N decreases by 0.4 and 0.5 G, respectively, i.e., of about 17% and 23% of the whole solvent effect. The further inclusion of dispersion terms does not affect the difference with FQ average values.

In order to best compare the results of our approach with experimental findings, DFT values were also corrected to account for some intrinsic deficiency. To this end, the difference between full DFT and full CCSD data obtained for clusters ($\Delta_{\text{CC/PBE0}}$, see Table IV) was added to the calculated QM/MM value. The resulting values are labeled “Best QM/MM” in Table VI. Remarkably, our best computed values are in excellent agreement with experimental data for both radicals, thus confirming the accuracy and reliability of our approach.

To get further insight into solvent effects on hcc_N values, differences between FQ and QM values are reported as a function of the snapshot in Fig. 7. As it can be noticed, for both PROXYL (top)

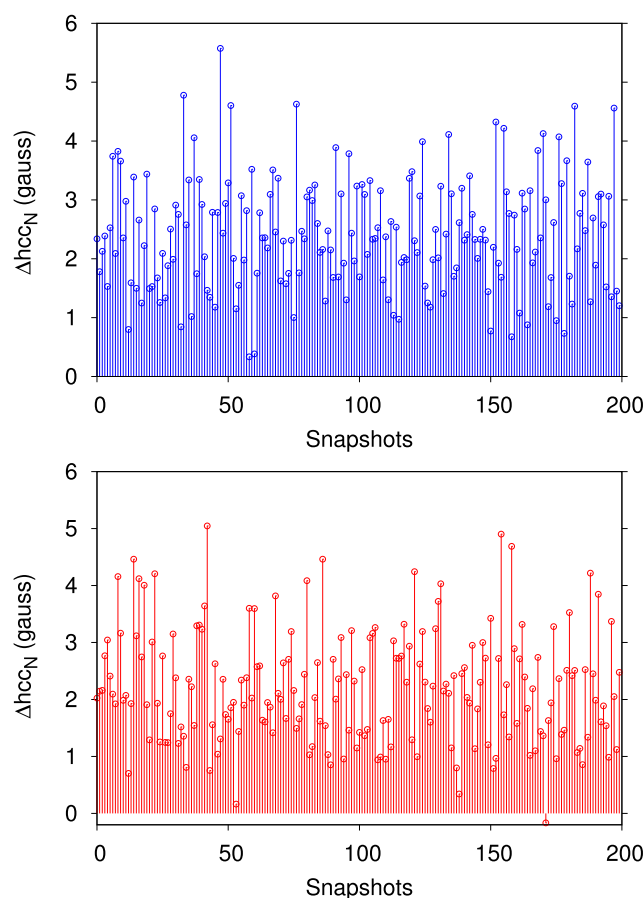


FIG. 7. Calculated solvent effects (see text) on hcc_N as a function of the snapshot extracted from MD runs (Top: PROXYL; bottom: TEMPO). All data are reported in Gauss.

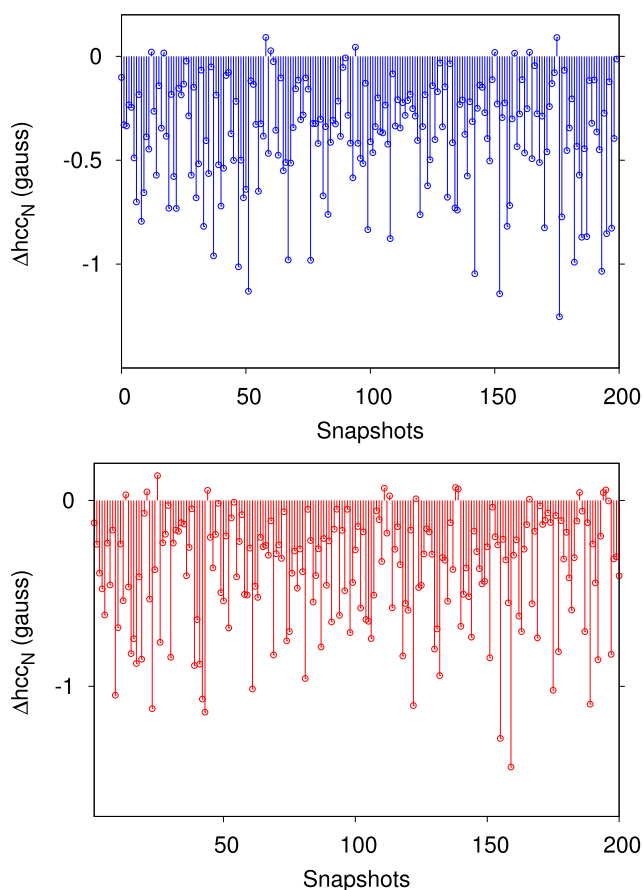


FIG. 8. Difference between FQ and QM/FQ+repulsion solvent effects as a function of the snapshot extracted from the MD (Top: PROXYL; bottom: TEMPO). All data are reported in Gauss.

and TEMPO (bottom), the electrostatic solvent contribution to hcc_N is always positive (only in one case, a small negative contribution is reported for TEMPO). Notice that this is different from what has been reported for electric properties of higher order.⁸⁴

In Fig. 8, the difference between calculated solvent effects on hcc_N as obtained with the purely electrostatic FQ approach or with the further inclusion of the repulsion contribution is reported. Remarkably, repulsion contributions increase or decrease the hcc_N value depending on the selected snapshot, thus showing that cluster approaches do not guarantee an adequate modeling of solvent effects. In fact, although repulsion effects give on average a negative contribution to hcc_N , by taking a random snapshot (cluster), a completely different picture could emerge.

V. SUMMARY AND CONCLUSIONS

In this paper, we have extended to the calculation of hyperfine coupling constants, the model proposed in Ref. 43 to include Pauli repulsion and dispersion effects in QM/MM approaches. The peculiarity of the proposed approach stands in the fact that repulsion/dispersion contributions are explicitly introduced in the QM

Hamiltonian. Therefore, such terms not only enter the evaluation of energetic properties but also, remarkably, propagate to molecular properties and spectra. The account of such contributions has permitted a quantitative analysis of QM/MM interaction energies, and this has also required a novel parametrization of the FQ force field, which has been then tested against the prediction of EPR hcc_N of PROXYL and TEMPO in aqueous solutions.

Numerical applications to the two radicals *in vacuo*, solvated within the so-called cluster approach or as modeled through MD, confirm the well known relevance of solvent effects and a proper account of their dynamical aspects. The further inclusion of dispersion and especially repulsion solute-solvent interactions gives, remarkably, an almost perfect agreement between calculated and experimental values. Therefore, although electrostatic effects have been invoked as dominating the solvation phenomenon in aqueous solution, we found that non-electrostatic effects are indeed relevant, contributing to 17% and 23% of the entire solvent effects on hcc_N for PROXYL and TEMPO, respectively. Remarkably, dispersion interactions seem not to play a crucial role.

To end the discussion, we remark that our model is general enough to be applied to any kind of solvent/environment, pending a reliable parametrization of both electrostatic and non-electrostatic interactions. Also, due to the inclusion of all terms in the molecular Hamiltonian, our approach can be extended to any kind of molecular properties and spectroscopies; this will be the topic of future communications.

SUPPLEMENTARY MATERIAL

See [supplementary material](#) for PBE0/N07D and CCSD/EPR-II reduced TEMPO hcc_N values as a function of the out of plane $C_\alpha NOC_\alpha$ angle. PROXYL and TEMPO selected geometrical parameters at different levels of theory with the inclusion of Grimme empirical dispersion D3. PROXYL+2w interaction energies calculated at the QM/FQ, SAPT0, and CCSD(T) level. O and H parameters for FQ calculations. PROXYL and TEMPO hcc_N calculated on 200 snapshots extracted from MD runs.

ACKNOWLEDGMENTS

We are thankful for the computer resources provided by the high performance computer facilities of the SMART Laboratory (<http://smart.sns.it/>). C.C. gratefully acknowledges the support of H2020-MSCA-ITN-2017 European Training Network “Computational Spectroscopy In Natural sciences and Engineering” (COSINE), Grant No. 765739.

REFERENCES

1. J. Tomasi, B. Mennucci, and R. Cammi, “Quantum mechanical continuum solvation models,” *Chem. Rev.* **105**, 2999–3094 (2005).
2. H. M. Senn and W. Thiel, “QM/MM methods for biomolecular systems,” *Angew. Chem., Int. Ed.* **48**, 1198–1229 (2009).
3. J. R. Cheeseman, M. S. Shaik, P. L. Popelier, and E. W. Blanch, “Calculation of Raman optical activity spectra of methyl- β -D-glucose incorporating a full molecular dynamics simulation of hydration effects,” *J. Am. Chem. Soc.* **133**, 4991–4997 (2011).
4. B. Mennucci, “Modeling environment effects on spectroscopies through QM/classical models,” *Phys. Chem. Chem. Phys.* **15**, 6583–6594 (2013).

- ⁵K. H. Hopmann, K. Ruud, M. Pecul, A. Kudelski, M. Dračinský, and P. Bour, "Explicit versus implicit solvent modeling of Raman optical activity spectra," *J. Phys. Chem. B* **115**, 4128–4137 (2011).
- ⁶C. Cappelli, F. Lipparini, J. Bloino, and V. Barone, "Towards an accurate description of anharmonic infrared spectra in solution within the polarizable continuum model: Reaction field, cavity field and nonequilibrium effects," *J. Chem. Phys.* **135**, 104505 (2011).
- ⁷F. Egidi, T. Giovannini, M. Piccardo, J. Bloino, C. Cappelli, and V. Barone, "Stereoelectronic, vibrational, and environmental contributions to polarizabilities of large molecular systems: A feasible anharmonic protocol," *J. Chem. Theory Comput.* **10**, 2456–2464 (2014).
- ⁸C. Cappelli, "Integrated QM/polarizable MM/continuum approaches to model chiroptical properties of strongly interacting solute-solvent systems," *Int. J. Quantum Chem.* **116**, 1532–1542 (2016).
- ⁹E. Boulanger and J. N. Harvey, "QM/MM methods for free energies and photochemistry," *Curr. Opin. Struct. Biol.* **49**, 72–76 (2018).
- ¹⁰P. Lahiri, K. B. Wiberg, P. H. Vaccaro, M. Caricato, and T. D. Crawford, "Large solvation effect in the optical rotatory dispersion of norbornene," *Angew. Chem.* **126**, 1410–1413 (2014).
- ¹¹D. Loco, S. Jurinovich, L. Cupellini, M. F. Menger, and B. Mennucci, "The modeling of the absorption lineshape for embedded molecules through a polarizable QM/MM approach," *Photochem. Photobiol. Sci.* **17**, 552–560 (2018).
- ¹²A. Warshel and M. Levitt, "Theoretical studies of enzymic reactions: Dielectric, electrostatic and steric stabilization of the carbonium ion in the reaction of lysozyme," *J. Mol. Biol.* **103**, 227–249 (1976).
- ¹³M. J. Field, P. A. Bash, and M. Karplus, "A combined quantum mechanical and molecular mechanical potential for molecular dynamics simulations," *J. Comput. Chem.* **11**, 700–733 (1990).
- ¹⁴J. Gao, "Hybrid quantum and molecular mechanical simulations: An alternative avenue to solvent effects in organic chemistry," *Acc. Chem. Res.* **29**, 298–305 (1996).
- ¹⁵R. A. Friesner and V. Guallar, "Ab initio quantum chemical and mixed quantum mechanics/molecular mechanics (QM/MM) methods for studying enzymatic catalysis," *Annu. Rev. Phys. Chem.* **56**, 389–427 (2005).
- ¹⁶H. Lin and D. G. Truhlar, "QM/MM: What have we learned, where are we, and where do we go from here?," *Theor. Chem. Acc.* **117**, 185–199 (2007).
- ¹⁷A. Monari, J.-L. Rivail, and X. Assfeld, "Theoretical modeling of large molecular systems. Advances in the local self consistent field method for mixed quantum mechanics/molecular mechanics calculations," *Acc. Chem. Res.* **46**, 596–603 (2012).
- ¹⁸A. Monari, T. Very, J.-L. Rivail, and X. Assfeld, "A QM/MM study on the spinach plastocyanin: Redox properties and absorption spectra," *Comput. Theor. Chem.* **990**, 119–125 (2012).
- ¹⁹P. N. Day, J. H. Jensen, M. S. Gordon, S. P. Webb, W. J. Stevens, M. Krauss, D. Garmer, H. Basch, and D. Cohen, "An effective fragment method for modeling solvent effects in quantum mechanical calculations," *J. Chem. Phys.* **105**, 1968–1986 (1996).
- ²⁰V. Kairys and J. H. Jensen, "QM/MM boundaries across covalent bonds: A frozen localized molecular orbital-based approach for the effective fragment potential method," *J. Phys. Chem. A* **104**, 6656–6665 (2000).
- ²¹Y. Mao, O. Demerdash, M. Head-Gordon, and T. Head-Gordon, "Assessing ion-water interactions in the amoeba force field using energy decomposition analysis of electronic structure calculations," *J. Chem. Theory Comput.* **12**, 5422–5437 (2016).
- ²²D. Loco, É. Polack, S. Caprasecca, L. Lagardere, F. Lipparini, J.-P. Piquemal, and B. Mennucci, "A QM/MM approach using the amoeba polarizable embedding: From ground state energies to electronic excitations," *J. Chem. Theory Comput.* **12**, 3654–3661 (2016).
- ²³D. Loco and L. Cupellini, "Modeling the absorption lineshape of embedded systems from molecular dynamics: A tutorial review," *Int. J. Quantum Chem.* **119**, e25726 (2019).
- ²⁴B. T. Thole, "Molecular polarizabilities calculated with a modified dipole interaction," *Chem. Phys.* **59**, 341–350 (1981).
- ²⁵A. H. Steindal, K. Ruud, L. Frediani, K. Aidas, and J. Kongsted, "Excitation energies in solution: The fully polarizable QM/MM/PCM method," *J. Phys. Chem. B* **115**, 3027–3037 (2011).
- ²⁶S. Jurinovich, C. Curutchet, and B. Mennucci, "The Fenna-Matthews-Olson protein revisited: A fully polarizable (TD) DFT/MM description," *ChemPhysChem* **15**, 3194–3204 (2014).
- ²⁷E. Boulanger and W. Thiel, "Solvent boundary potentials for hybrid QM/MM computations using classical drude oscillators: A fully polarizable model," *J. Chem. Theory Comput.* **8**, 4527–4538 (2012).
- ²⁸S. W. Rick, S. J. Stuart, and B. J. Berne, "Dynamical fluctuating charge force fields: Application to liquid water," *J. Chem. Phys.* **101**, 6141–6156 (1994).
- ²⁹S. W. Rick and B. J. Berne, "Dynamical fluctuating charge force fields: The aqueous solvation of amides," *J. Am. Chem. Soc.* **118**, 672–679 (1996).
- ³⁰T. Giovannini, M. Olszówka, F. Egidi, J. R. Cheeseman, G. Scalmani, and C. Cappelli, "Polarizable embedding approach for the analytical calculation of Raman and Raman optical activity spectra of solvated systems," *J. Chem. Theory Comput.* **13**, 4421–4435 (2017).
- ³¹F. Lipparini, F. Egidi, C. Cappelli, and V. Barone, "The optical rotation of methyloxirane in aqueous solution: A never ending story?," *J. Chem. Theory Comput.* **9**, 1880–1884 (2013).
- ³²D. Loco, F. Buda, J. Lugtenburg, and B. Mennucci, "The dynamic origin of color tuning in proteins revealed by a carotenoid pigment," *J. Phys. Chem. Lett.* **9**, 2404–2410 (2018).
- ³³J. E. Lennard-Jones, "Cohesion," *Proc. Phys. Soc.* **43**, 461 (1931).
- ³⁴E. Boulanger, L. Huang, C. Rupakheti, A. D. MacKerell, Jr., and B. Roux, "Optimized Lennard-Jones parameters for druglike small molecules," *J. Chem. Theory Comput.* **14**, 3121–3131 (2018).
- ³⁵M. S. Gordon, Q. A. Smith, P. Xu, and L. V. Slipchenko, "Accurate first principles model potentials for intermolecular interactions," *Annu. Rev. Phys. Chem.* **64**, 553–578 (2013).
- ³⁶H. Gokcan, E. G. Kratz, T. A. Darden, J.-P. Piquemal, and G. A. Cisneros, "QM/MM simulations with the Gaussian electrostatic model, a density-based polarizable potential," *J. Phys. Chem. Lett.* **9**, 3062–3067 (2018).
- ³⁷M. S. Gordon, L. Slipchenko, H. Li, and J. H. Jensen, "The effective fragment potential: A general method for predicting intermolecular interactions," *Annu. Rep. Comput. Chem.* **3**, 177–193 (2007).
- ³⁸M. S. Gordon, M. A. Freitag, P. Bandyopadhyay, J. H. Jensen, V. Kairys, and W. J. Stevens, "The effective fragment potential method: A QM-based MM approach to modeling environmental effects in chemistry," *J. Phys. Chem. A* **105**, 293–307 (2001).
- ³⁹I. Adamovic and M. S. Gordon, "Dynamic polarizability, dispersion coefficient C_6 and dispersion energy in the effective fragment potential method," *Mol. Phys.* **103**, 379–387 (2005).
- ⁴⁰L. V. Slipchenko, "Effective fragment potential method," in *Many-Body Effects and Electrostatics in Biomolecules* (Pan Stanford, 2016), pp. 147–187.
- ⁴¹J. M. H. Olsen, C. Steinmann, K. Ruud, and J. Kongsted, "Polarizable density embedding: A new QM/QM/MM-based computational strategy," *J. Phys. Chem. A* **119**, 5344–5355 (2015).
- ⁴²P. Reinholdt, J. Kongsted, and J. M. H. Olsen, "Polarizable density embedding: A solution to the electron spill-out problem in multiscale modeling," *J. Phys. Chem. Lett.* **8**, 5949–5958 (2017).
- ⁴³T. Giovannini, P. Lafiosca, and C. Cappelli, "A general route to include Pauli repulsion and quantum dispersion effects in QM/MM approaches," *J. Chem. Theory Comput.* **13**, 4854–4870 (2017).
- ⁴⁴A. Tkatchenko and M. Scheffler, "Accurate molecular van der Waals interactions from ground-state electron density and free-atom reference data," *Phys. Rev. Lett.* **102**, 073005 (2009).
- ⁴⁵A. Tkatchenko, L. Romaner, O. T. Hofmann, E. Zojer, C. Ambrosch-Draxl, and M. Scheffler, "Van der Waals interactions between organic adsorbates and at organic/inorganic interfaces," *MRS Bull.* **35**, 435–442 (2010).
- ⁴⁶A. Tkatchenko, R. A. DiStasio, Jr., R. Car, and M. Scheffler, "Accurate and efficient method for many-body van der Waals interactions," *Phys. Rev. Lett.* **108**, 236402 (2012).

- ⁴⁷J. Hermann, R. A. DiStasio, and A. Tkatchenko, "First-principles models for van der Waals interactions in molecules and materials: Concepts, theory, and applications," *Chem. Rev.* **117**, 4714–4758 (2017).
- ⁴⁸C. Curutchet, L. Cupellini, J. Kongsted, S. Corni, L. Frediani, A. H. Stein-dal, C. A. Guido, G. Scalmani, and B. Mennucci, "Density-dependent formulation of dispersion–repulsion interactions in hybrid multiscale quantum/molecular mechanics (QM/MM) models," *J. Chem. Theory Comput.* **14**, 1671–1681 (2018).
- ⁴⁹G. A. Cisneros, J.-P. Piquemal, and T. A. Darden, "Intermolecular electrostatic energies using density fitting," *J. Chem. Phys.* **123**, 044109 (2005).
- ⁵⁰J.-P. Piquemal, G. A. Cisneros, P. Reinhardt, N. Gresh, and T. A. Darden, "Towards a force field based on density fitting," *J. Chem. Phys.* **124**, 104101 (2006).
- ⁵¹G. A. Cisneros, J.-P. Piquemal, and T. A. Darden, "Generalization of the Gaussian electrostatic model: Extension to arbitrary angular momentum, distributed multipoles, and speedup with reciprocal space methods," *J. Chem. Phys.* **125**, 184101 (2006).
- ⁵²M. Pavone, P. Cimino, F. De Angelis, and V. Barone, "Interplay of stereoelectronic and environmental effects in tuning the structural and magnetic properties of a prototypical spin probe: Further insights from a first principle dynamical approach," *J. Am. Chem. Soc.* **128**, 4338–4347 (2006).
- ⁵³V. Barone, "Electronic, vibrational and environmental effects on the hyperfine coupling constants of nitroxide radicals. H₂NO as a case study," *Chem. Phys. Lett.* **262**, 201–206 (1996).
- ⁵⁴R. Improta and V. Barone, "Interplay of electronic, environmental, and vibrational effects in determining the hyperfine coupling constants of organic free radicals," *Chem. Rev.* **104**, 1231–1254 (2004).
- ⁵⁵M. Pavone, P. Cimino, O. Crescenzi, A. Sillanpää, and V. Barone, "Interplay of intrinsic, environmental, and dynamic effects in tuning the EPR parameters of nitroxides: Further insights from an integrated computational approach," *J. Phys. Chem. B* **111**, 8928–8939 (2007).
- ⁵⁶V. Barone, P. Cimino, O. Crescenzi, and M. Pavone, "Ab initio computation of spectroscopic parameters as a tool for the structural elucidation of organic systems," *J. Mol. Struct.: THEOCHEM* **811**, 323–335 (2007).
- ⁵⁷M. Pavone, A. Sillanpää, P. Cimino, O. Crescenzi, and V. Barone, "Evidence of variable H-bond network for nitroxide radicals in protic solvents," *J. Phys. Chem. B* **110**, 16189–16192 (2006).
- ⁵⁸V. Barone, M. Brustolon, P. Cimino, A. Polimeno, M. Zerbetto, and A. Zoleo, "Development and validation of an integrated computational approach for the modeling of cw-ESR spectra of free radicals in solution: *p*-(methylthio) phenyl nitronitroxide in toluene as a case study," *J. Am. Chem. Soc.* **128**, 15865–15873 (2006).
- ⁵⁹E. Stendardo, A. Pedone, P. Cimino, M. C. Menziani, O. Crescenzi, and V. Barone, "Extension of the amber force-field for the study of large nitroxides in condensed phases: An *ab initio* parameterization," *Phys. Chem. Chem. Phys.* **12**, 11697–11709 (2010).
- ⁶⁰V. Barone, P. Cimino, and A. Pedone, "An integrated computational protocol for the accurate prediction of EPR and PNMN parameters of aminoxyl radicals in solution," *Magn. Reson. Chem.* **48**, S11–S22 (2010).
- ⁶¹J. C. Schöneboom, F. Neese, and W. Thiel, "Toward identification of the compound I reactive intermediate in cytochrome P450 chemistry: A QM/MM study of its EPR and Mössbauer parameters," *J. Am. Chem. Soc.* **127**, 5840–5853 (2005).
- ⁶²S. Sinnecker and F. Neese, "QM/MM calculations with DFT for taking into account protein effects on the EPR and optical spectra of metalloproteins. Plastocyanin as a case study," *J. Comput. Chem.* **27**, 1463–1475 (2006).
- ⁶³S. Moon, S. Patchkovskii, and D. R. Salahub, "QM/MM calculations of EPR hyperfine coupling constants in blue copper proteins," *J. Mol. Struct.: THEOCHEM* **632**, 287–295 (2003).
- ⁶⁴H. M. Senn and W. Thiel, "QM/MM studies of enzymes," *Curr. Opin. Chem. Biol.* **11**, 182–187 (2007).
- ⁶⁵V. Barone, A. Bencini, M. Cossi, A. D. Matteo, M. Mattesini, and F. Totti, "Assessment of a combined QM/MM approach for the study of large nitroxide systems *in vacuo* and in condensed phases," *J. Am. Chem. Soc.* **120**, 7069–7078 (1998).
- ⁶⁶L. J. Berliner, *Spin Labeling: Theory and Applications* (Academic, New York, 1976).
- ⁶⁷N. Kocherginsky and H. M. Swartz, *Nitroxide Spin Labels: Reactions in Biology and Chemistry* (CRC Press, New York, 1995).
- ⁶⁸A. H. Buchaklian and C. S. Klug, "Characterization of the walker a motif of MsbA using site-directed spin labeling electron paramagnetic resonance spectroscopy," *Biochemistry* **44**, 5503–5509 (2005).
- ⁶⁹M. Engström, O. Vahtras, and H. Ågren, "MCSCF and DFT calculations of EPR parameters of sulfur centered radicals," *Chem. Phys. Lett.* **328**, 483–491 (2000).
- ⁷⁰Z. Rinkevicius, B. Frecus, N. A. Murugan, O. Vahtras, J. Kongsted, and H. Ågren, "Encapsulation influence on EPR parameters of spin-labels: 2, 2, 6, 6-tetramethyl-4-methoxypiperidine-1-oxyl in cucurbit[8]uril," *J. Chem. Theory Comput.* **8**, 257–263 (2011).
- ⁷¹K. J. de Almeida, Z. Rinkevicius, H. W. Hugosson, A. C. Ferreira, and H. Ågren, "Modeling of EPR parameters of copper (II) aqua complexes," *Chem. Phys.* **332**, 176–187 (2007).
- ⁷²C. Di Valentin, G. Pacchioni, A. Selloni, S. Livraghi, and E. Giamello, "Characterization of paramagnetic species in N-doped TiO₂ powders by EPR spectroscopy and DFT calculations," *J. Phys. Chem. B* **109**, 11414–11419 (2005).
- ⁷³M. Anpo, Y. Shioya, H. Yamashita, E. Giamello, C. Morterra, M. Che, H. H. Patterson, S. Webber, and S. Ouellette, "Preparation and characterization of the Cu⁺/zsm-5 catalyst and its reaction with NO under UV irradiation at 275 K. *In situ* photoluminescence, EPR, and FT-IR investigations," *J. Phys. Chem.* **98**, 5744–5750 (1994).
- ⁷⁴J.-L. Clément, N. Ferré, D. Siri, H. Karoui, A. Rockenbauer, and P. Tordo, "Assignment of the EPR spectrum of 5, 5-dimethyl-1-pyrroline *N*-oxide (DMPO) superoxide spin adduct," *J. Org. Chem.* **70**, 1198–1203 (2005).
- ⁷⁵E. Giner, L. Tenti, C. Angeli, and N. Ferré, "Computation of the isotropic hyperfine coupling constant: Efficiency and insights from a new approach based on wave function theory," *J. Chem. Theory Comput.* **13**, 475–487 (2017).
- ⁷⁶C. Amovilli and R. McWeeny, "A matrix partitioning approach to the calculation of intermolecular potentials. General theory and some examples," *Chem. Phys.* **140**, 343–361 (1990).
- ⁷⁷R. McWeeny, *Methods of Molecular Quantum Mechanics* (Academic Press, London, 1992).
- ⁷⁸F. Lipparini and V. Barone, "Polarizable force fields and polarizable continuum model: A fluctuating charges/PCM approach. 1. Theory and implementation," *J. Chem. Theory Comput.* **7**, 3711–3724 (2011).
- ⁷⁹F. Lipparini, C. Cappelli, G. Scalmani, N. De Mitri, and V. Barone, "Analytical first and second derivatives for a fully polarizable QM/classical Hamiltonian," *J. Chem. Theory Comput.* **8**, 4270–4278 (2012).
- ⁸⁰T. Giovannini, M. Olszowka, and C. Cappelli, "Effective fully polarizable QM/MM approach to model vibrational circular dichroism spectra of systems in aqueous solution," *J. Chem. Theory Comput.* **12**, 5483–5492 (2016).
- ⁸¹T. Giovannini, G. Del Frate, P. Lafioca, and C. Cappelli, "Effective computational route towards vibrational optical activity spectra of chiral molecules in aqueous solution," *Phys. Chem. Chem. Phys.* **20**, 9181–9197 (2018).
- ⁸²T. Giovannini, M. Macchiagodena, M. Ambrosetti, A. Puglisi, P. Lafioca, G. Lo Gerfo, F. Egidi, and C. Cappelli, "Simulating vertical excitation energies of solvated dyes: From continuum to polarizable discrete modeling," *Int. J. Quantum Chem.* **119**, e25684 (2019).
- ⁸³F. Lipparini, C. Cappelli, and V. Barone, "Linear response theory and electronic transition energies for a fully polarizable QM/classical Hamiltonian," *J. Chem. Theory Comput.* **8**, 4153–4165 (2012).
- ⁸⁴T. Giovannini, M. Ambrosetti, and C. Cappelli, "A polarizable embedding approach to second harmonic generation (SHG) of molecular systems in aqueous solutions," *Theor. Chem. Acc.* **137**, 74 (2018).
- ⁸⁵C. Amovilli and B. Mennucci, "Self-consistent-field calculation of Pauli repulsion and dispersion contributions to the solvation free energy in the polarizable continuum model," *J. Phys. Chem. B* **101**, 1051–1057 (1997).
- ⁸⁶F. L. Hirshfeld, "Bonded-atom fragments for describing molecular charge densities," *Theor. Chem. Acc.* **44**, 129–138 (1977).
- ⁸⁷I. Harczuk, B. Nagy, F. Jensen, O. Vahtras, and H. Ågren, "Local decomposition of imaginary polarizabilities and dispersion coefficients," *Phys. Chem. Chem. Phys.* **19**, 20241–20250 (2017).
- ⁸⁸S. Grimme, "Density functional theory with London dispersion corrections," *Wiley Interdiscip. Rev.: Comput. Mol. Sci.* **1**, 211–228 (2011).

- ⁸⁹S. Grimme, J. Antony, S. Ehrlich, and H. Krieg, "A consistent and accurate *ab initio* parametrization of density functional dispersion correction (DFT-D) for the 94 elements H-Pu," *J. Chem. Phys.* **132**, 154104 (2010).
- ⁹⁰O. L. Malkina, J. Vaara, B. Schimmelpfennig, M. Munzarová, V. G. Malkin, and M. Kaupp, "Density functional calculations of electronic g-tensors using spin-orbit pseudopotentials and mean-field all-electron spin-orbit operators," *J. Am. Chem. Soc.* **122**, 9206–9218 (2000).
- ⁹¹M. Kaupp, C. Remenyi, J. Vaara, O. L. Malkina, and V. G. Malkin, "Density functional calculations of electronic g-tensors for semiquinone radical anions. The role of hydrogen bonding and substituent effects," *J. Am. Chem. Soc.* **124**, 2709–2722 (2002).
- ⁹²V. Barone and P. Cimino, "Accurate and feasible computations of structural and magnetic properties of large free radicals: The PBE0/N07D model," *Chem. Phys. Lett.* **454**, 139–143 (2008).
- ⁹³V. Barone, P. Cimino, and E. Stendardo, "Development and validation of the B3LYP/N07D computational model for structural parameter and magnetic tensors of large free radicals," *J. Chem. Theory Comput.* **4**, 751–764 (2008).
- ⁹⁴V. Barone, "Structure, magnetic properties and reactivities of open-shell species from density functional and self-consistent hybrid methods," in *Recent Advances in Density Functional Methods: Part I* (World Scientific, 1995), pp. 287–334.
- ⁹⁵R. M. Parrish, L. A. Burns, D. G. A. Smith, A. C. Simmonett, A. E. DePrince, E. G. Hohenstein, U. Bozkaya, A. Y. Sokolov, R. Di Remigio, R. M. Richard, J. F. Gonthier, A. M. James, H. R. McAlexander, A. Kumar, M. Saitow, X. Wang, B. P. Pritchard, P. Verma, H. F. Schaefer, K. Patkowski, R. A. King, E. F. Valeev, F. A. Evangelista, J. M. Turney, T. D. Crawford, and C. D. Sherrill, "Psi4 1.1: An open-source electronic structure program emphasizing automation, advanced libraries, and interoperability," *J. Chem. Theory Comput.* **13**, 3185–3197 (2017).
- ⁹⁶P. Mark and L. Nilsson, "Structure and dynamics of the TIP3P, SPC, and SPC/E water models at 298 K," *J. Phys. Chem. A* **105**, 9954–9960 (2001).
- ⁹⁷I. Carnimeo, C. Cappelli, and V. Barone, "Analytical gradients for MP2, double hybrid functionals, and TD-DFT with polarizable embedding described by fluctuating charges," *J. Comput. Chem.* **36**, 2271–2290 (2015).
- ⁹⁸V. Hornak, R. Abel, A. Okur, B. Strockbine, A. Roitberg, and C. Simmerling, "Comparison of multiple amber force fields and development of improved protein backbone parameters," *Proteins* **65**, 712–725 (2006).
- ⁹⁹D. A. Case, T. E. Cheatham, T. Darden, H. Gohlke, R. Luo, K. M. Merz, A. Onufriev, C. Simmerling, B. Wang, and R. J. Woods, "The amber biomolecular simulation programs," *J. Comput. Chem.* **26**, 1668–1688 (2005).
- ¹⁰⁰J.-P. Ryckaert, G. Ciccotti, and H. J. Berendsen, "Numerical integration of the Cartesian equations of motion of a system with constraints: Molecular dynamics of *n*-alkanes," *J. Comput. Phys.* **23**, 327–341 (1977).
- ¹⁰¹T. Darden, D. York, and L. Pedersen, "Particle mesh Ewald: An $N \log(N)$ method for Ewald sums in large systems," *J. Chem. Phys.* **98**, 10089–10092 (1993).
- ¹⁰²M. J. Frisch, G. W. Trucks, H. B. Schlegel, G. E. Scuseria, M. A. Robb, J. R. Cheeseman, G. Scalmani, V. Barone, G. A. Petersson, H. Nakatsuji, X. Li, M. Caricato, A. V. Marenich, J. Bloino, B. G. Janesko, R. Gomperts, B. Mennucci, H. P. Hratchian, J. V. Ortiz, A. F. Izmaylov, J. L. Sonnenberg, D. Williams-Young, F. Ding, F. Lipparini, F. Egidi, J. Goings, B. Peng, A. Petrone, T. Henderson, D. Ranasinghe, V. G. Zakrzewski, J. Gao, N. Rega, G. Zheng, W. Liang, M. Hada, M. Ehara, K. Toyota, R. Fukuda, J. Hasegawa, M. Ishida, T. Nakajima, Y. Honda, O. Kitao, H. Nakai, T. Vreven, K. Throssell, J. A. Montgomery, Jr., J. E. Peralta, F. Ogliaro, M. J. Bearpark, J. J. Heyd, E. N. Brothers, K. N. Kudin, V. N. Staroverov, T. A. Keith, R. Kobayashi, J. Normand, K. Raghavachari, A. P. Rendell, J. C. Burant, S. S. Iyengar, J. Tomasi, M. Cossi, J. M. Millam, M. Klene, C. Adamo, R. Cammi, J. W. Ochterski, R. L. Martin, K. Morokuma, O. Farkas, J. B. Foresman, and D. J. Fox, Gaussian 16, Revision A.03, Gaussian Inc., Wallingford, CT, 2016.
- ¹⁰³J. F. Keana, T. D. Lee, and E. M. Bernard, "Side-chain substituted 2, 2, 5, 5-tetramethylpyrrolidine-N-oxyl (proxyl) nitroxides. A new series of lipid spin labels showing improved properties for the study of biological membranes," *J. Am. Chem. Soc.* **98**, 3052–3053 (1976).
- ¹⁰⁴A. Rockenbauer, L. Korecz, and K. Hideg, "Ring pseudorotation in pyrrolidine N-oxyl radicals: An analysis of ¹³C-hyperfine structure of EPR spectra," *J. Chem. Soc., Perkin Trans. 2* **0**(11), 2149–2156 (1993).
- ¹⁰⁵C. Puzzarini and V. Barone, "Diving for accurate structures in the ocean of molecular systems with the help of spectroscopy and quantum chemistry," *Acc. Chem. Res.* **51**, 548–556 (2018).
- ¹⁰⁶K. Szalewicz, "Symmetry-adapted perturbation theory of intermolecular forces," *Wiley Interdiscip. Rev.: Comput. Mol. Sci.* **2**, 254–272 (2012).
- ¹⁰⁷E. G. Hohenstein and C. D. Sherrill, "Wavefunction methods for non-covalent interactions," *Wiley Interdiscip. Rev.: Comput. Mol. Sci.* **2**, 304–326 (2012).
- ¹⁰⁸T. M. Parker, L. A. Burns, R. M. Parrish, A. G. Ryno, and C. D. Sherrill, "Levels of symmetry adapted perturbation theory (SAPT). I. Efficiency and performance for interaction energies," *J. Chem. Phys.* **140**, 094106 (2014).
- ¹⁰⁹S. F. Boys and F. d. Bernardi, "The calculation of small molecular interactions by the differences of separate total energies. Some procedures with reduced errors," *Mol. Phys.* **19**, 553–566 (1970).